NANO MICRO small

Supporting Information

for *Small*, DOI: 10.1002/smll.201903572

Thermodynamically Stable Mesoporous C_3N_7 and C_3N_6 with Ordered Structure and Their Excellent Performance for Oxygen Reduction Reaction

In Young Kim, Sungho Kim, Selvarajan Premkumar, Jae-Hun Yang, Siva Umapathy, and Ajayan Vinu**

Supporting Information

Thermodynamically Stable Mesoporous C_3N_7 and C_3N_6 with Ordered Structure and Their Excellent Performance for Oxygen Reduction Reaction

In Young Kim,[†] Sungho Kim,[†] Selvarajan Premkumar, Jae-Hun Yang, Siva Umapathy and Ajayan Vinu**

Experimental details

Preparation of KIT-6 template: KIT-6 was synthesized via the typical method previously reported.[1] In brief, 4 g of Pluronic P123 was dipersed in 144 g of deionized water and 7.9 g of 36wt% HCl, followed by stirring the mixture for 3 h at 35 ^{o}C. After that, 4.0 g of n-butanol was added into the solution, which was stirring for further 1 h at 35 ^{o}C. 8.0 g of tetraethyl orthosilicate (TEOS) was added drop by drop to the mixed solution and kept at the same temperature for 24 h. The solution was transferred to the Teflon lined autoclave and aged for 24 h at 150 °C. Then, the sample was filtered without washing and dried for 24 h at 100 ^{o}C. The dried sample was calcined at 540 °C under air atmosphere for 12 h.

Preparation of reference materials of triazole-based C_3N_5 and g-C_3N_4: The mesoporous and bulk triazole-based C_3N_5 were synthesized by pyrolysis of 5-amino-1H-tetrazole at a temperature of 400 ^{o}C with/witout KIT-6 template as previously reported.[2] Bulk g-C_3N_4 was prepared according to a method in literature that is a calcination of dicyandiamide at 600 ^{o}C.[3]

Characterization: Thermogravimetric analysis of 5-ATTZ was carried out under N_2 atmosphere in a temperature range of 30–700 ^{o}C with a ramping rate of 10 ^{o}Cmin^{-1}. For relative thermal stability test, the mesoporous C_3N_7, C_3N_6, C_3N_5 and bulk g-C_3N_4 were annealed for 2 h at 250 ^{o}C and further heated up to 800 ^{o}C with a ramping rate of 5 ^{o}Cmin^{-1} under N_2 atmosphere. The chemical composition of the present materials

was determined by CHN analysis. A Leco CHN analyser was used to determine the amount of carbon and nitrogen in the carbon nitrides. A diffuse reflectance UV-Vis spectrometer was used to analyse bandgap of materials. The obtained UV-Vis reflectance spectra were converted to UV-Vis absorption spectra by the Kubelka-Munk equation. The powder X-ray diffraction (XRD) analysis was done using a Panalytical diffractometer with Cu K_α (λ=1.5418 Å) radiation produced at 40 kV and 40 mA. The high-resolution transmission electron microscopic (HR-TEM) images and electron diffraction patterns were captured on a Jeol JEM-2100F electron microscope. The N_2 adsorption-desorption isotherms were measured with Micromeritics ASAP 2420. Before the analysis, the samples were degassed by heat treatment under vacuum (10^{-3} torr) for 12 h at 200 °C. The surface areas and pore size of the materials were calculated through BET and BJH equations, respectively. Fourier transform infrared (FTIR) spectra were recorded with transmittance mode from 4000 to 400 cm^{-1} using the Malvern FTIR spectrometer. Near-edge X-ray absorption fine structure (NEXAFS) measurement was carried out on the Soft X-ray Spectroscopy Beamline at the Australian Synchrotron. The beamline has a hemispherical electron analyser and a microchannel plate detector in order to measure the total electron yield and partial electron yield simultaneously. The normalization of raw NEXAFS data were undertaken by the photoelectron current of the photon beam, generated on an Au grid. The theoretical NEXAFS spectrum for the cluster with 3 Å radius was calculated using FDMNES code.[4] The micro-Raman spectra were recorded at room temperature using a commercial Raman micro-spectrometer (Renishaw, InVia system). A diode laser having 830 nm line was used as the excitation source.

Electrocatalytic activity test for ORR: The potentials were converted to reversible hydrogen electrode (RHE) scale with following equation: $E_{RHE} = E_{Ag/AgCl}+0.059pH+E°_{Ag/AgCl}$. The kinetic current density and electron transfer number

were calculated through the K-L equation. Based on the K-L theory, the current density behaviour on RDE is described as follows:

$$1/j = 1/j_k + 1/j_L = 1/B\times\omega^{-1/2} + 1/j_k$$

where j, j_k and j_L are defined as the measured, kinetic-limited, and mass-transfer-limited current densities, respectively. Since j_k is proportional to the square root of angular velocity (ω) of the RDE, the proportionality coefficient (B) is

$$B=0.62D^{2/3}\nu^{-1/6}nFC^*$$

where D, ν, F and C^* are the diffusion coefficient of the reactant, kinematic viscosity of the electrolyte, Faraday constant and concentration of the reactant in the bulk electrolyte, respectively. Thus, n can be inferred from the slope of the linear plot of j^{-1} vs. $\omega^{-1/2}$ (K-L plot).

Table S1. CHN analysis results of the carbon nitride samples.

Sample	Carbon (wt%)	Nitrogen (wt%)	Carbon (at%)	Nitrogen (at%)	N/C atomic ratio
C_3N_7	23.16	59.89	1.93	4.28	2.23
C_3N_6	25.93	56.71	2.16	4.05	1.87
C_3N_5	27.96	54.26	2.33	3.87	1.66
g-C_3N_4	31.96	52.56	2.66	3.75	1.41

A quantitative CHN analysis is the most appropriate technique to determine chemical composition of carbon nitride. Based on the CHN analysis, chemical composition of the prepared materials has been determined as $C_3N_{6.7}$ ($\approx C_3N_7$), $C_3N_{5.6}$ ($\approx C_3N_6$), $C_3N_{5.0}$ ($\approx C_3N_5$) and $C_3N_{4.23}$ ($\approx C_3N_4$).

Table S2. Textural parameters of the C_3N_7 and C_3N_6.

	BET surface area (m^2g^{-1})	**Pore diameter (nm)**	**Total pore volume (cm^3g^{-1})**
C_3N_7	114	4.4	0.19
C_3N_6	167	3.3	0.22

Table S3. Comparison of ORR activity of pure carbon nitrides and their carbon composites.

Electrocatalysts	Morphology	Carbon content	Onset potential (*E* vs RHE)	Electrolytes	References
ordered mesoporous C_3N_7	3D ordered mesoporous	not applicable	0.81 V	0.1 M KOH	In this work
ordered mesoporous C_3N_6	3D ordered mesoporous	not applicable	0.80 V	0.1M KOH	In this work
ordered mesoporous C_3N_5	3D ordered mesoporous	not applicable	0.78 V	0.1M KOH	[2]
ordered mesoporous g-C_3N_4	ordered mesoporous	not applicable	0.75 V	0.1 M $HClO_4$	[5]
bulk g-C_3N_4	bulk	not applicable	0.74 V	0.1M KOH	In this work
1D g-C_3N_4	1D tubular nanostructure	not applicable	0.81 V	0.1M KOH	[6]
ordered mesoporous C_3N_5-graphene hybrid	3D ordered mesoporous	1.96wt%	0.81 V	0.1 M KOH	[2]
3D ordered macroporous g-C_3N_4/carbon composite	macroporous	54wt%	0.84 V	0.1 M KOH	[7]
g-C_3N_4@CMK-3 composites	nanoporous	72.9wt%	0.86 V	0.1M KOH	[8]
crystalline carbon-conjugated g-C_3N_4	nanosheet	not reported	0.95 V	0.1 M KOH	[9]

Figure S1. TGA graphs of 5-ATTZ under N_2 atmosphere.

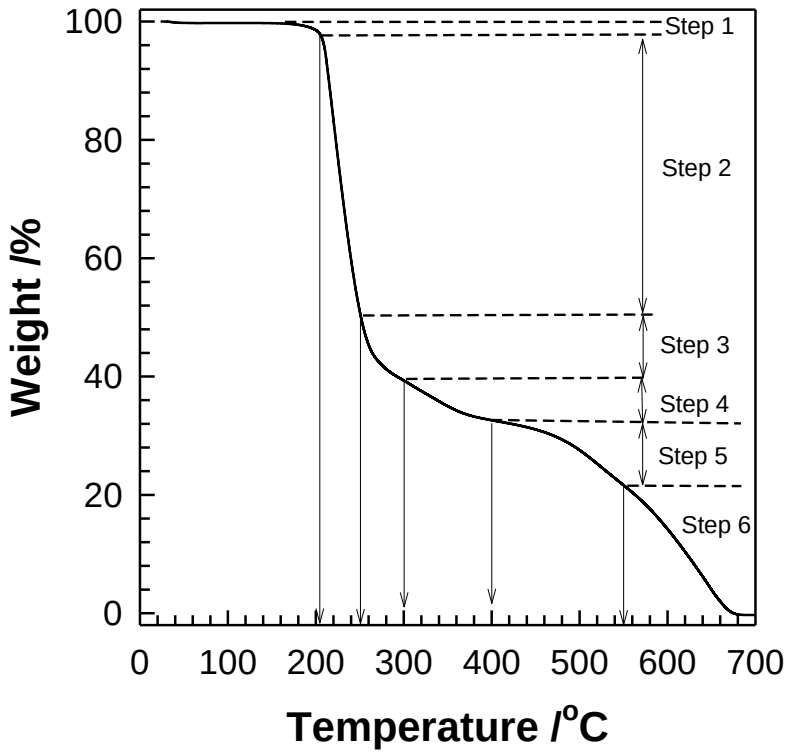

A small weight loss between 30 and 205 ^{o}C corresponds to a removal of water adsorbed (step 1). Melting point of 5-ATTZ is 205 ^{o}C and it is decomposed to cyanamide (CH_2N_2) and hydrazoic acid (N_3H) after melting.[10] It is known that pyrolysis processes of 5-ATTZ at 400 and 550 ^{o}C produce triazole-based C_3N_5 (step 4) and g-C_3N_4 (step 5), respectively.[2],[10] Finally the carbon nitrides are completely decomposed at 700 ^{o}C (step 6). A significant weight loss between 205 and 400 ^{o}C is attributed to loss of elements upon a polymerization of the cyanamide and hydrazoic acid. To the best of our knowledge, there is no study on intermediate products derived from 5-ATTZ via low temperature-pyrolysis, which is important to confirm possibilities of existence of N-rich carbon nitrides such as C_3N_7 and C_3N_6. Thus, temperatures of 250 and 300 ^{o}C were chosen for polymerization mechanism study of 5-ATTZ at low temperature (step 2 and 3).

Figure S2. UV-Vis light absorption spectra of the triazole-based mesoporous (i) C_3N_7 and (ii) C_3N_6 with the reference material of (iii) triazole-based mesoporous C_3N_5.

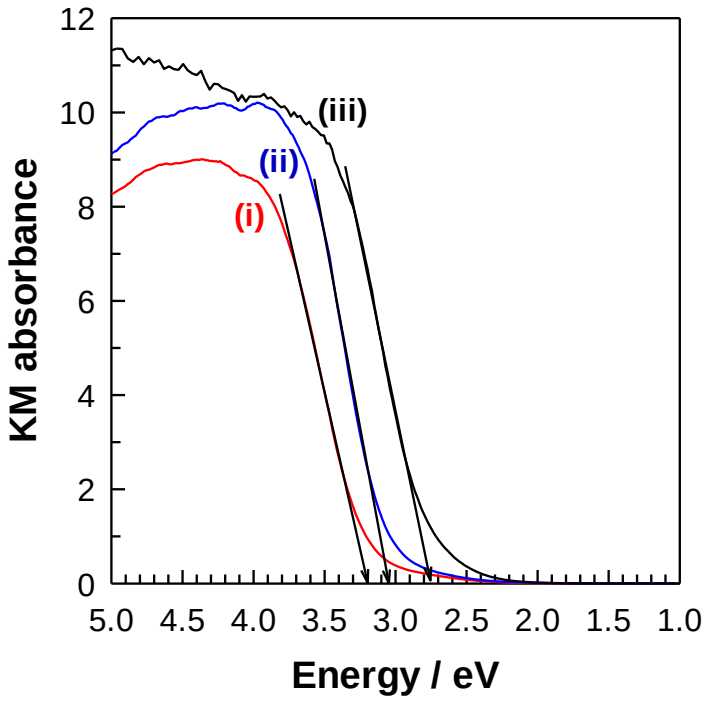

Figure S3. TGA graphs of the mesoporous C_3N_7, C_3N_6, C_3N_5 and bulk g-C_3N_4 under N_2 atmosphere.

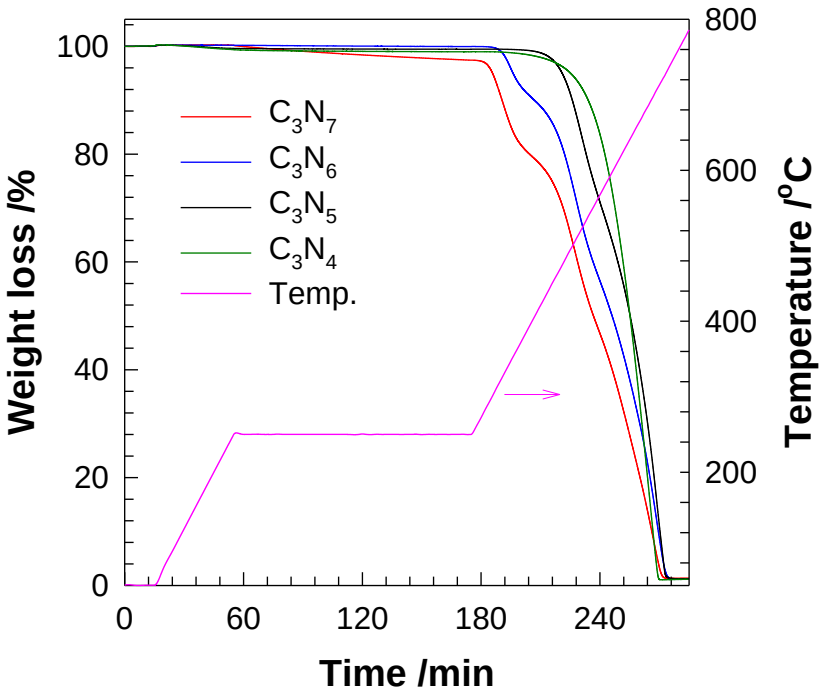

Relative thermal stability of the mesoporous C_3N_7 and C_3N_6 was evaluated with reference materials of the mesoporous C_3N_5 and bulk g-C_3N_4 by TGA analysis. While the prgrammed temperature was maintained at 250 ^oC for 2 h, the C_3N_7, C_3N_6, and C_3N_5 and g-C_3N_4 show small weight losses of 2.74, 0.24, 0.14 and 0.40wt% , respectively. Although the mesoporous C_3N_7 displays the largest weight loss among the present samples, its weight loss of only 2.74wt% suggests that the C_3N_7 is quite thermodynamically stable at 250 ^oC. The relative thermal stability of the present materials also can be determined with a characteristic temperature occuring 50% weight loss ($T_{50\%}$). The $T_{50\%}$ of the C_3N_7, C_3N_6, C_3N_5 and g-C_3N_4 is 551, 597, 642 and 642 ^oC, respectively.

Figure S4. (Left) N_2 adsorption-desorption isotherms and (right) BJH pore size distribution curves of the triazole-based mesoporous (i) C_3N_7 and (ii) C_3N_6.

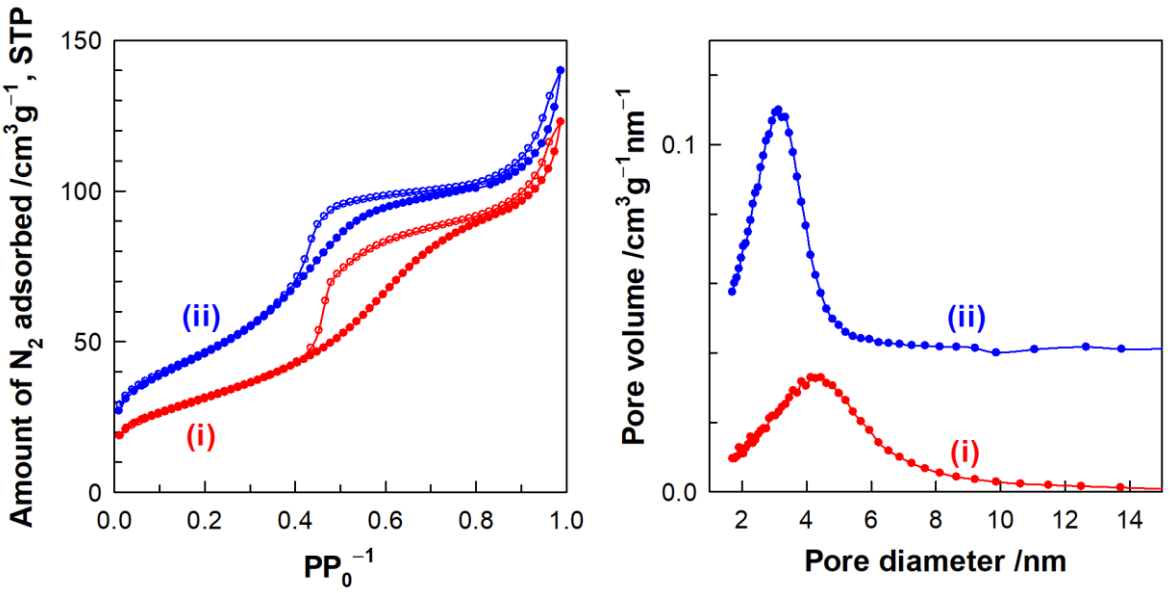

Figure S5. Micro-Raman spectra of (i) bulk C_3N_7, (ii) mesoporous C_3N_7, (iii) bulk C_3N_6, (iv) mesoporous C_3N_6 with reference materials of (v) bulk triazole-based C_3N_5 and (vi) g-C_3N_4.

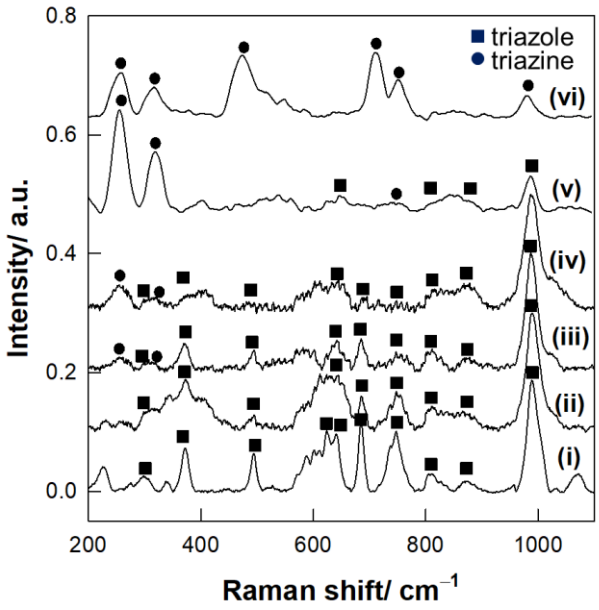

Micro-Raman spectra of bulk and mesoporous C_3N_7 and C_3N_6 were compared with bulk triazole-based C_3N_5 and C_3N_6. It is confirmed that the Raman spectra of mesoporous C_3N_7 and C_3N_6 are identical to those of bulk C_3N_7 and C_3N_6. The circles and squares denoted in the spectra indicate Raman bands originated from triazine and triazole moieties, respectively.[2],[11] While g-C_3N_4 shows Raman bands at 261, 321, 476, 714, 756 and 984 cm^{-1}, C_3N_7 exhibits Raman bands at 302, 373, 496, 624, 643, 686, 748, 809, 870 and 991 cm^{-1}. The tendency is clearly seen, which is that triazole features are diminished and triazine features become stronger as N content increases in present carbon nitrides.

Figure S6. Proposed phase transition mechanism of 5-ATTZ

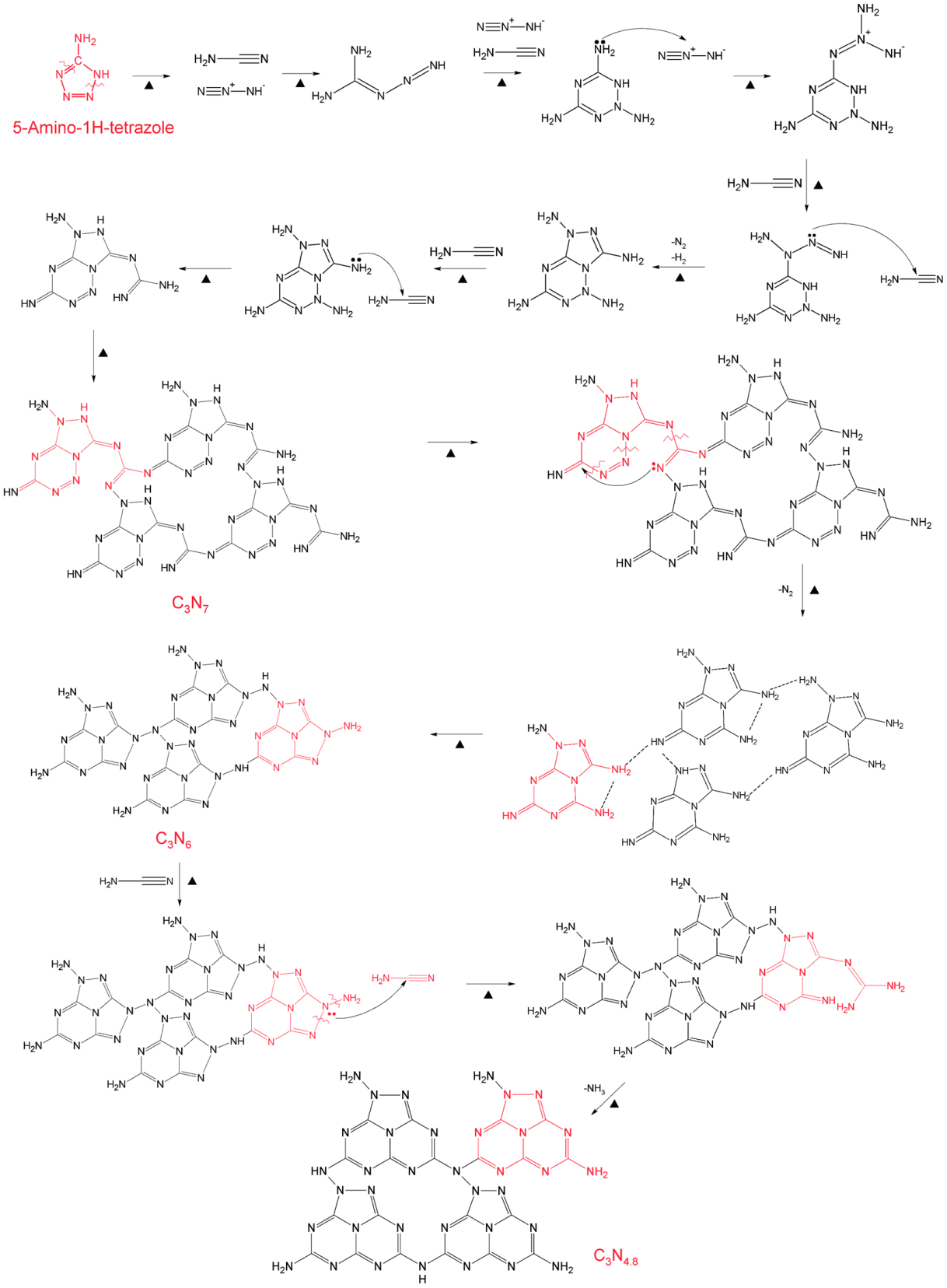

Figure S7. LSV of the (i) Vulcan C, (ii) Vulcan C-free C_3N_6 and (iii) Vulcan C-free C_3N_7.

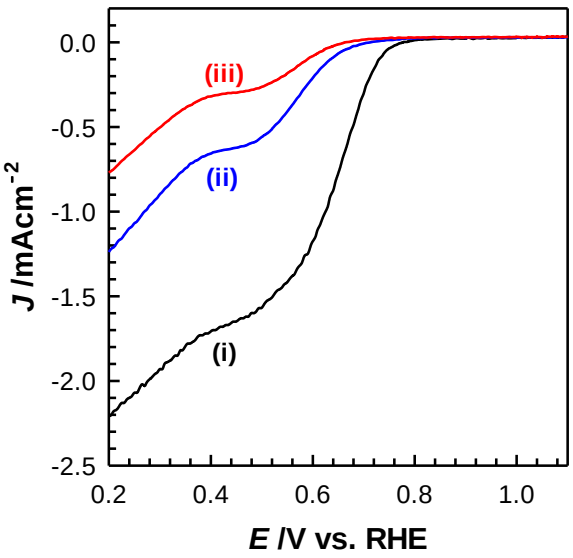

As carbon black itself has a certain degree of ORR activity under alkaline conditions, ORR activities of the Vulcan C-free mesoporous C_3N_7 and Vulcan C-free mesoporous C_3N_6 and Vulcan C. As shown in Figure S7, all the materials exhibit certain ORR activities under 0.1 M KOH solution, but those are much less than ORR activities of the C_3N_7 and C_3N_6 with Vulcan C (**Figure 3a)**. This study suggests that ORR activities of the C_3N_7 and C_3N_6 shown in **Figure 3a** are not originated from the Vulcan C and highlights an importance of improvement of electronic conductivity of carbon nitride to have high ORR activity.

Figure S8. Phonon DOS of the C_3N_7.

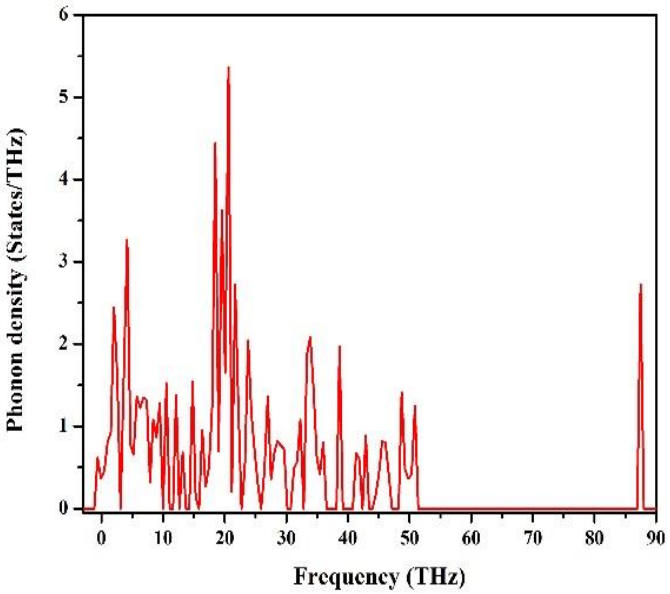

Thermodynamic stability of a material can be evaluated by a sign of frequencies in phonon density of states (DOS) through DFT calculations. All the positive frequencies in phonon DOS of the C_3N_7 provide an evidence that the proposed structure of the C_3N_7 is thermodynamically stable.

Figure S9. (Left) Partial DOS and (right) band diagram of the C_3N_7.

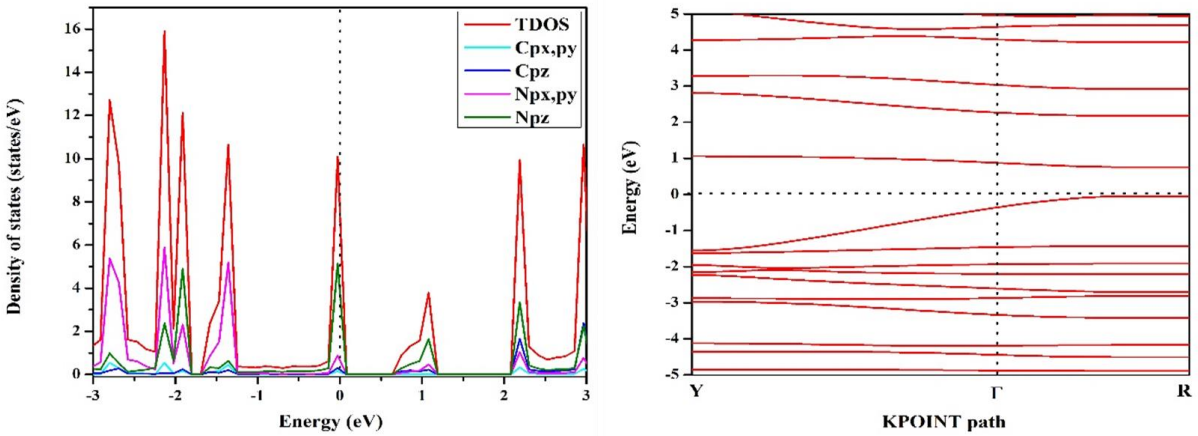

Partial density of states (PDOS) of the C_3N_7 indicates that both valence and conduction bands are dominated by N_{pz} electrons. Theoretically predicted DOS of the C_3N_7 reveals that the system has energy gap of 0.82 eV. Band structure diagram of the C_3N_7 shows that maximum of both valence and conduction bands locates at Γ. This indicates that the C_3N_7 is a direct semiconductor.

Figure S10. Comparison between N K-edge NEXAFS experimental spectrum of the mesoporous C_3N_7 and theoretical spectrum calculated with the proposed C_3N_7 model.

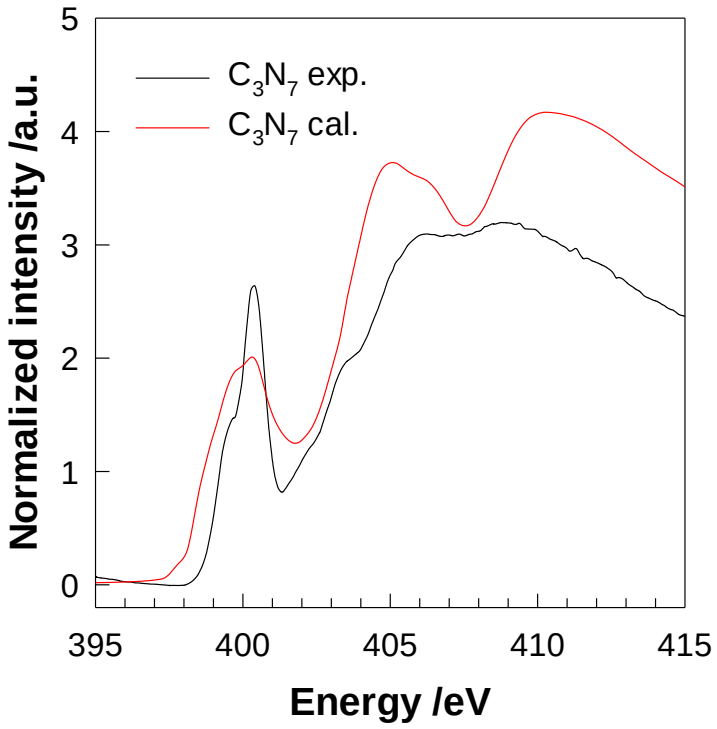

Figure S11. (Left) two-dimensional and (right) three-dimensional electron density distribution map of the C_3N_7.

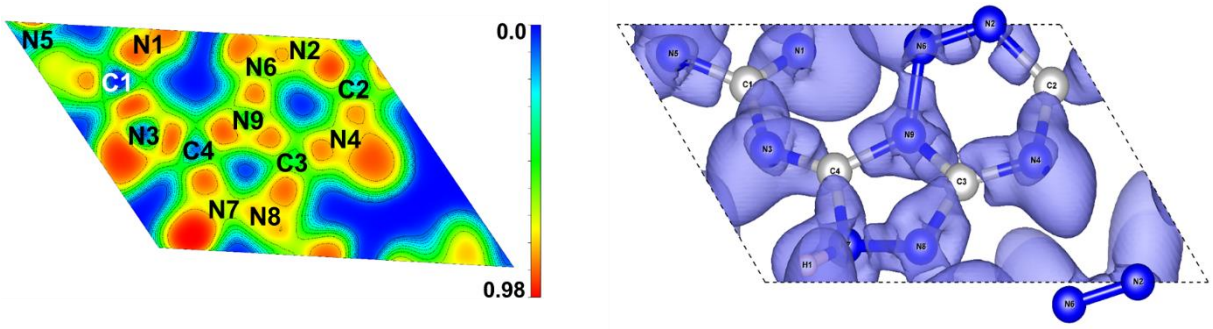

References for Supporting Information

[1] F. Kleitz, S. H. Choi, R. Ryoo, *Chem. Commun.* **2003**, 2136.

[2] I. Y. Kim, S. Kim, X. Jin, S. Premkumar, G. Chandra, N. -S. Lee, G. P. Mane, S. -J. Hwang, S. Umapathy and A. Vinu, *Angew. Chem. Int. Ed.* **2018**, *57*, 17135-17140.

[3] X. Ju, K. Xu, P. Chen, K. Jia, S. Liu, C. Wu, *J. Mater. Chem. A* **2014**, *2*, 18924.

[4] O. Bunau, Y. Joly, *J. Phys.: Condens. Matter.* **2009**, *21*, 345501.

[5] K. Kwon, Y. J. Sa, J. Y. Cheon, S. H. Joo, *Langmuir* **2012**, *28*, 991-996.

[6] M. Tahir, N. Mahmood, J. Zhu, A. Mahmood, F. K. Butt, S. Rizwan, I. Aslam, M. Tanveer, F. Idrees, I. Shakir, C. Cao, Y. Hou, *Sci. Rep.* **2015**, *5*, 12389.

[7] J. Liang, Y. Zheng, J. Chen, J. Liu, D. Hulicova-Jurcakova, M. Jaroniec, S. Z. Qiao, *Angew. Chem. Int. Ed.* **2012**, *51*, 3892-3896.

[8] Y. Zheng, Y. Jiao, J. Chen, J. Liu, J. Liang, A. Du, W. Zhang, Z. Zhu, S. C. Smith, M. Jaroniec, G. Q. Lu, S. Z. Qiao, *J. Am. Chem. Soc.* **2011**, *133*, 20116-20119.

[9] W. Niu, K. Marcus, L. Zhou, Z. Li, L. Shi, K. Liang, Y. Yang, *ACS Catal.* **2018**, *8*, 1926-1931.

[10] A. Savateev, S. Pronkin, J. D. Epping, M. G. Willinger, C. Wolff, D. Neher, M. Antonietti, D. Dontsova, *ChemCatChem* **2017**, *9*, 167-174.

[11] Q. Xiang, J. Yu, M. Jaroniec, *J. Phys. Chem. C* **2011**, *115*, 7355-7363.